Effect of IMF B_Y on thermospheric composition at high and middle latitudes:
1. Numerical experiments

G. Crowley,[1,2] T. J. Immel,[3] C. L. Hackert,[1] J. Craven,[4] and R. G. Roble[5]

[1]   Magnetic storms and their effects on the thermosphere and ionosphere have been studied for many years, yet there are many aspects of the thermospheric and ionospheric responses that are not understood. The purpose of this paper is to show how the high-latitude composition depends on the sign of the IMF B_Y component, using controlled simulations with a global first principles model. Because the high-latitude convection and neutral wind systems are strongly controlled by the IMF B_Y component, it seems likely that the compositional response that is driven by high-latitude forcing should also be sensitive to the B_Y component. To date, no first-principles modeling has been performed to test the idea of IMF B_Y effects on composition. Numerical experiments using model simulations provide insight into this important scientific question, since the thermospheric compositional response to the convection patterns for different IMF B_Z and B_Y can be studied in isolation in a model. In this paper we use a first-principles model to determine the effect of the IMF B_Y component on the compositional response of the high-latitude thermosphere. We show for the first time that a clockwise rotation of the potential pattern resulting from a change from B_Y-negative to B_Y-positive drives a corresponding rotation in the wind, neutral density, and composition distributions. B_Y control of thermospheric composition has been invoked in the literature to explain an apparent variability in the effectiveness of auroral activity in causing thermospheric storm effects at middle latitudes, as observed in global images of the far-ultraviolet (FUV) OI 130.4-nm emission from the DE-1 auroral imager. However, the effect in the simulations presented here is opposite from that suggested by earlier work based on DE data, indicating another explanation must be sought for the DE results. These simulations are highly relevant for interpreting data being provided by more modern UV imaging instruments on the DMSP, TIMED, and IMAGE satellites.

1.   Scientific Background

[2]   Magnetic storms and substorms cause major changes in the compositional distribution of the thermosphere. There have been numerous studies of the compositional and density response to high-latitude forcing. Until recently, these studies were mostly a form of exploratory science, based on sparse in situ satellite data [e.g., *Hedin et al.*, 1977; *Miller et al.*, 1990]. However a picture emerged of upwelling molecular-rich air at high latitudes, with transport to lower latitudes on the nightside, followed by corotation [*Prölss*, 1980]. Even when in situ measurements of the atmospheric response were available from the Atmosphere Explorer (AE) and Dynamics Explorer-2 (DE-2) satellites, the high-latitude drivers were not generally measured globally in sufficient detail to specify model inputs. In addition, there have been detailed modeling studies [e.g., *Mayr and Volland*, 1973; *Crowley et al.*, 1989a, 1989b; *Burns et al.*, 1991, 1995a, 1995b; *Fuller-Rowell et al.*, 1994, 1996] that have confirmed and elucidated this picture. *Crowley et al.* [1989a, 1989b] confirmed that changes in thermospheric composition develop during storms and that Joule heating leads to upwelling of nitrogen-rich air that is transported to lower latitudes by equatorward winds on the nightside. Corotation then carries the oxygen-depleted air onto the dayside. *Burns et al.* [1991] described simulations that revealed upwelling and downwelling neutral winds as the primary mechanism causing the large enhancements of O relative to N_2 on the nightside in the winter hemisphere. Modeling by *Fuller-Rowell et al.* [1996] demonstrated the seasonal dependence of these processes and their effect on ionospheric electron

[1]Southwest Research Institute, San Antonio, Texas, USA.
[2]Now at Atmospheric and Space Technology Research Associates, San Antonio, Texas, USA.
[3]Space Sciences Laboratory, University of California, Berkeley, Berkeley, California, USA.
[4]Geophysical Institute and Physics Department, University of Alaska Fairbanks, Fairbanks, Alaska, USA.
[5]High Altitude Observatory, National Center for Atmospheric Research, Boulder, Colorado, USA.

densities. Much of this work was summarized by *Buonsanto* [1999]. In spite of the previous work, there remain many important science questions to be addressed regarding the atmospheric response to geomagnetic activity. The purpose of this paper is to show how the high-latitude composition depends on the sign of the IMF B_Y component, using controlled simulations with a global first-principles model.

[3] The strong influence of the IMF B_Y and B_Z components on ionospheric electric fields and ion convection in the high-latitude regions is well known. For periods of negative IMF B_Z, the configuration of the high-latitude, two-cell convection pattern is affected by the sign and magnitude of B_Y, while the cross polar cap potential is affected by the magnitude of B_Z [*Reiff et al.*, 1981; *Doyle and Burke*, 1983]. This B_Y effect on ion convection was first described by *Heppner* [1972], later by *Heelis* [1984], and more recently by *Ruohonemi and Greenwald* [1995] and *Weimer* [1996]. For increasingly positive (negative) B_Y, the Northern Hemisphere dusk (dawn) convection cell increases in size relative to its counterpart and the electric field also grows stronger in the dusk (dawn) cell. The corresponding effect of B_Y on the potential patterns for northward B_Z were measured by *Crowley et al* [1992], who showed that the convection configuration depends on the ratio of B_Y/B_Z.

[4] Through ion-neutral coupling, the IMF components also influence the circulation of neutrals at high latitudes. *McCormac et al.* [1985], *Thayer et al.* [1987], and *McCormac et al.* [1991] used neutral wind measurements from the low-altitude Dynamics Explorer 2 (DE-2) satellite to investigate the B_Y dependence of the neutral circulation. The IMF influence on polar cap neutral winds in the Northern Hemisphere was also described by *Killeen et al.* [1995] using ground-based Fabry-Perot interferometers (FPIs). For positive (negative) B_Y, both the size of the northern dusk (dawn) circulation cell and the corresponding neutral wind speeds increase; this is similar to the B_Y effect on the ion convection patterns. *Rees et al.* [1986] showed that the transition of the auroral zonal winds from westward to eastward in the midnight sector occurs about 2 hours earlier for B_Y negative than for B_Y positive, according to ground-based FPI measurements from Kiruna. In the Southern Hemisphere, the effect is similar except that the dawn (dusk) cell is enhanced with positive (negative) B_Y [*Hernandez et al.*, 1991]. For the Southern Hemisphere, *Thayer et al.* [1987] found that the antisunward winds were rotated from the noon-midnight meridian 7° toward dusk for B_Y positive, but 15° toward dawn for B_Y negative.

[5] The B_Y dependence of the neutral wind has also been investigated with thermospheric models such as UCL's 3D-TD [*Rees et al.*, 1985] and the NCAR TGCM [*Roble et al.*, 1988]. In each of these studies, the models were run for IMF conditions observed in late 1981 and early 1982 when thermospheric neutral winds and other properties were simultaneously measured by instruments aboard DE 2. The Roble et al. results were for a period of positive B_Y, resulting in simulation results showing high-speed antisunward flow in the postmidnight sector of the northern polar cap that is associated with an enhanced clockwise dusk circulation vortex. These observations compared well to the DE-2 data available for that period. The UCL results of *Rees et al.* [1986] show, for

periods of IMF B_Y positive, that the antisunward winds carry neutral gas into a region of the postmidnight sector where strong equatorward directed winds (out of the polar cap) dominate.

[6] An important development in the dynamics and structure of the high-latitude thermosphere was the discovery [*Crowley et al.*, 1989a, 1989b] of an organized density cell structure in the neutral thermosphere at high latitudes. The structure consists of two to four high- and low-density regions having diameters of 1000 to 2000 km. The number, location, and amplitude of the density cells depend on magnetic activity level and altitude. Below 170 km altitudes, only two cells are ever present, regardless of the magnitude of cross-cap potential from 30 to 120 kV. Above about 170 km, as geomagnetic activity increases, the two-cell pattern grows to multiple cells. Under magnetically quiet conditions, only two high-latitude cells are present. The high-density region (referred to as the noon cell) is most often located in or near the noon sector, although it sometimes protrudes into the midnight sector for certain UTs. The lower-density cell is always located in the morning sector (dawn cell). At 200 km, for a 60 kV cross cap potential, there are typically three cells; the additional cell is a high-density cell in the midnight sector. For magnetically active conditions ($\sim$90 kV cross cap potential), the neutral mass density at 200 km forms four high-latitude cells. The dawn cell for active conditions is in a similar location to that found in the 30 and 60 kV cases. However, the noon and midnight high-density cells are separated by a low-density region over the pole referred to as the "dusk low-density cell." These earlier studies showed that the density cells are a dynamical feature driven by high-latitude momentum forcing, and they are organized in magnetic coordinates (like the electric potential pattern) rather than geographic coordinates. Thus, like the potential pattern, the density cells precess around the geographic pole in 24 hours.

[7] The mass-density in each cell is either enhanced or depleted from the hemispheric average by up to 30%, and larger perturbations are produced with larger forcing. The structure is thus a significant feature of the near-Earth space environment at high latitudes and suggests that a satellite sampling a fixed altitude might encounter density variations of 50% or more during geomagnetically active intervals, as it crosses the high-latitude region. The morphology of the density cells for equinox solar minimum conditions was investigated by *Crowley et al.* [1996a, 1996b] and for solar maximum conditions by *Schoendorf et al.* [1996a, 1996b], using the NCAR TIGCM (a predecessor to the TIME-GCM). Evidence for the predicted cellular structure was found in satellite data from the S85-1 satellite [*Crowley et al.*, 1995, 1996b], the SETA-1 satellites [*Schoendorf et al.*, 1996a], and the ESRO-4 satellite [*Caspers and Prölss*, 1999].

[8] Because the high-latitude convection and neutral wind systems are strongly controlled by the IMF B_Y component, it seems likely that the neutral density response and the compositional response underlying the total mass density structures, both of which are driven by high-latitude forcing and dynamics, should also be sensitive to the B_Y component. This topic provides the focus for the rest of this paper.

Day 267, 1981 (B$_Y$ ~ +10 nT)   Day 279, 1981 (B$_Y$ ~ 0 nT)
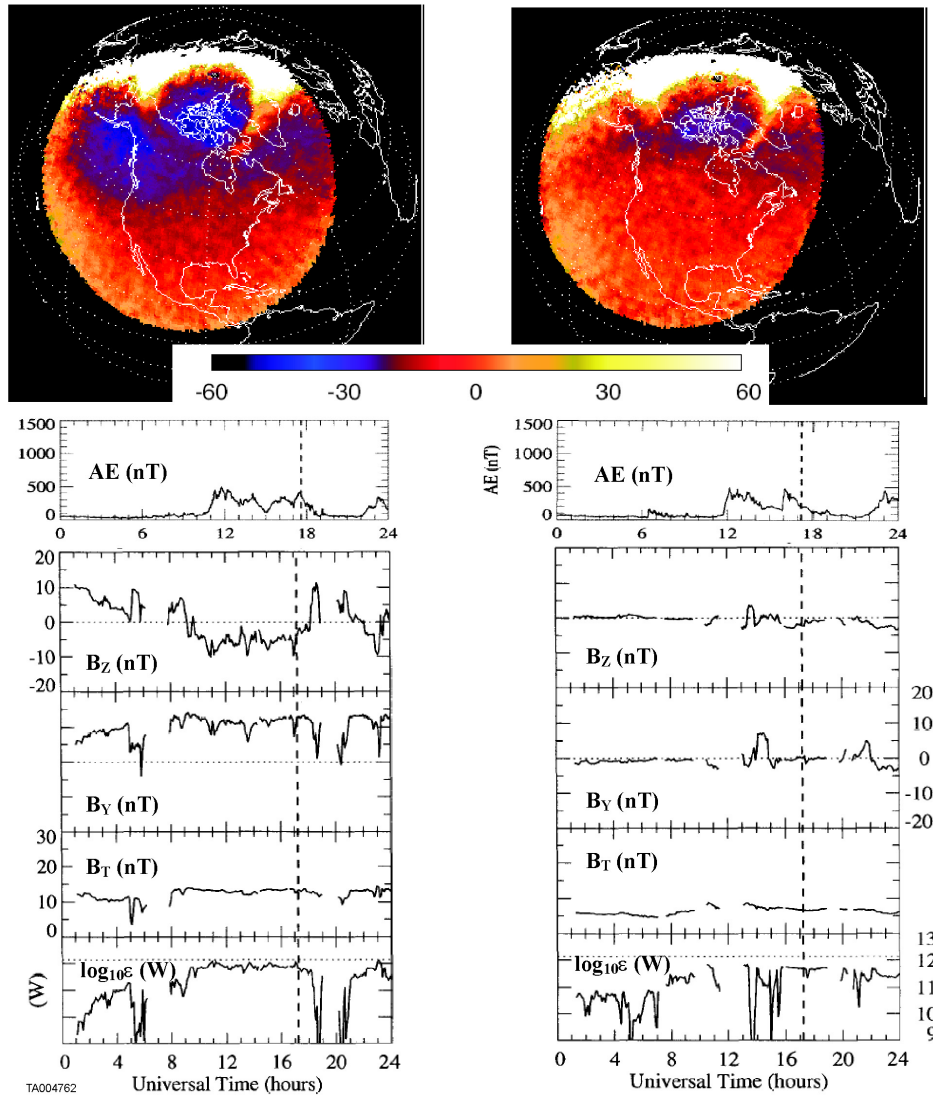
**Figure 1.** DE-1 FUV percentage deviation from quiet time (see text) for ~1700 UT on (a) Day 267 and (b) Day 279, 1981 (after *Immel et al.* [1997]). Lower panels show the corresponding AE index, IMF components (B$_Z$, B$_Y$, B$_T$), and the epsilon parameter for each day.

[9] Airglow images from space have been used to determine the column integrated O/N$_2$ ratio (ΣO/N$_2$) in the thermosphere, above about 135 km. Several authors have interpreted depletions in the 1304Å airglow observed from the DE-1 spacecraft as a reduction in ΣO/N$_2$ [e.g., *Craven et al.*, 1994; *Meier et al.*, 1995; *Immel et al.*, 2001]. *Strickland et al.* [2001] correlated changes in the critical frequency of the F2-region (foF2) with the ΣO/N$_2$ from the DE-1 satellite. Because the dayside F-region ionospheric electron density depends on the local O/N$_2$ number density ratio, the measurement of ΣO/N$_2$ offers an important parameter with which to constrain global model simulations of the composition and F-region electron density. B$_Y$ control of thermospheric composition was invoked by *Immel et al.* [1997] to explain an apparent variability in the effectiveness of auroral activity in causing thermospheric storm effects at middle latitudes, as observed in global images of the far-

ultraviolet (FUV) OI 130.4-nm emission provided by the DE-1 auroral imager.

[10] Figure 1 (after *Immel et al.* [1997]) shows DE-1 FUV images for ~1700 UT on days 267 and 279, 1981. The quiet-day FUV background has been subtracted, and the difference is shown as percentage variations from the quiet time. These are Northern Hemisphere images, mapped to geographic coordinates, centered at 50°N and the noon meridian, with morning at the left in each mapped image. The lower panels show the corresponding AE index, IMF (B$_Z$, B$_Y$, and B$_T$), and the Epsilon parameter indicating the flow of solar wind energy into the magnetosphere. Each image was obtained during and after a period of moderate magnetic activity.

[11] In Figure 1, image A (Day 267) shows a deep dayglow depletion extending from the morning terminator into the afternoon and including a portion of the polar cap,
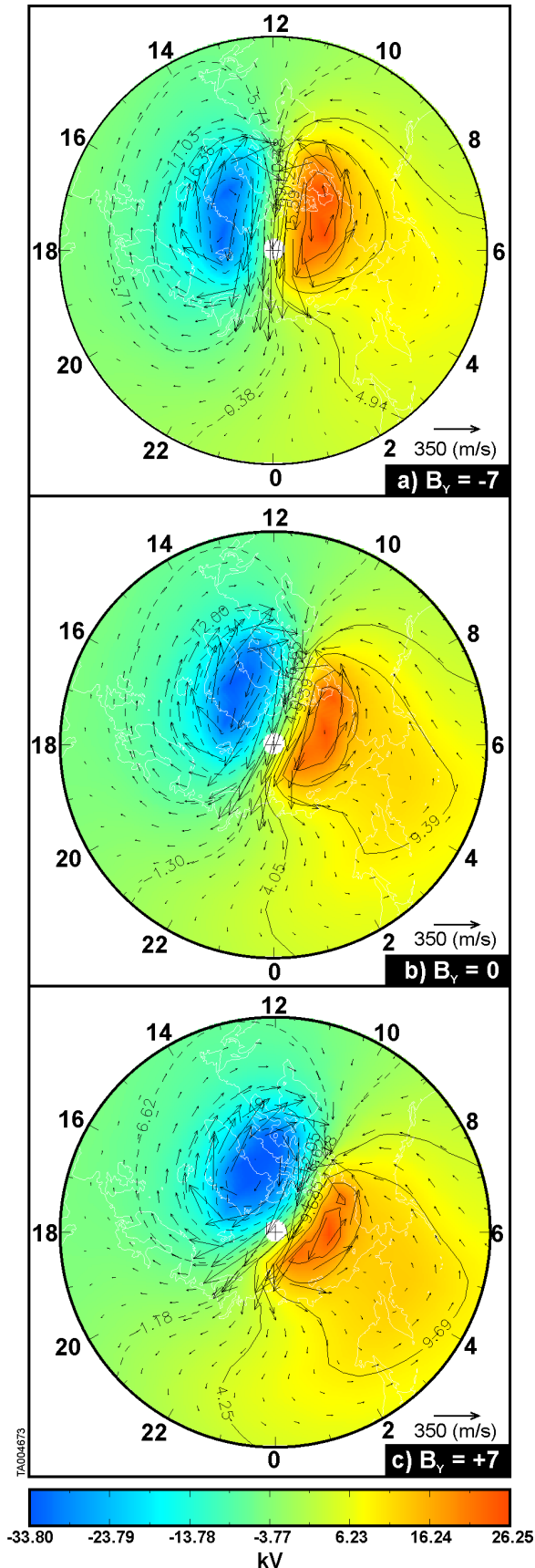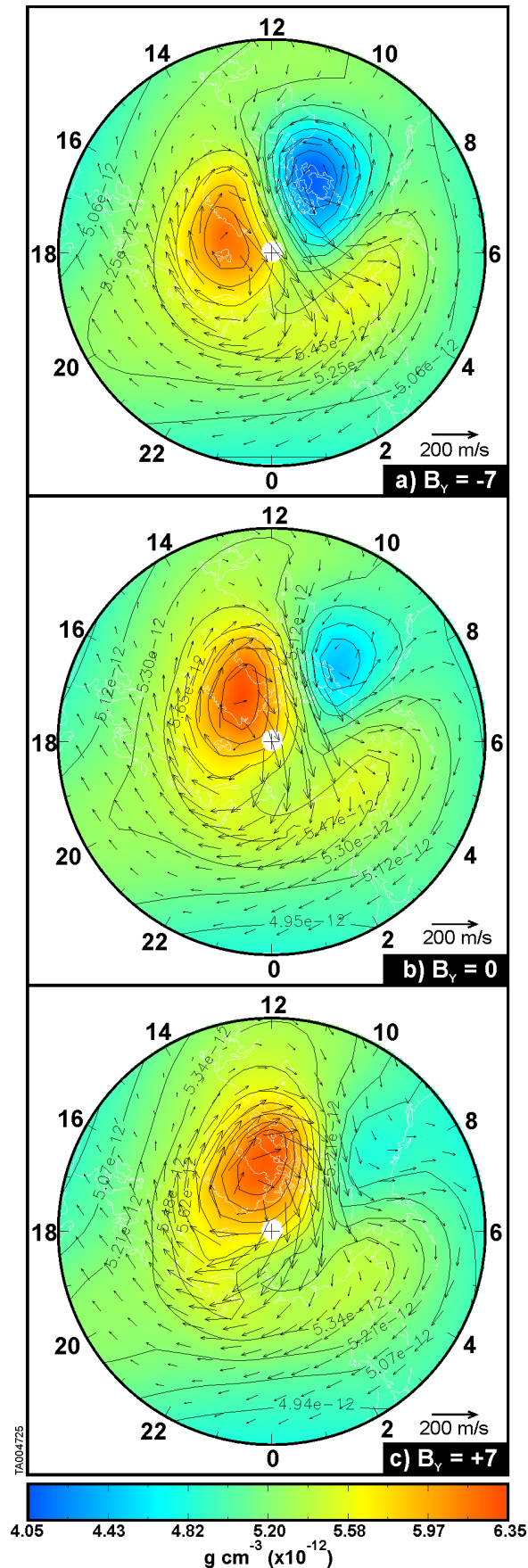
indicating significant reduction of the $\Sigma O/N_2$ ratio in the thermosphere. In the morning sector, the area of 20% decrease extends as far as 38°N, while the area of 10% decrease is observed to extend equatorward of 30°N. In contrast, image B (Day 279) shows a much smaller area of decreased dayglow brightness in the polar cap and the afternoon sector, with 10% decreases reaching down to only 50° geographic latitude. Smaller decreases are seen to extend to only about 60° latitude in the morning sector. The AE forcing history for Day 279 was remarkably similar to Day 267, leading to the question of how the composition responses could therefore be so different. *Immel et al.* [1997] suggested that the B_Y component was responsible for the difference. The IMF B_Y data in Figure 1 suggest that the appearance of strong disturbances in dayside composition in the Northern Hemisphere may be favored during periods of positive B_Y. *Immel et al.* [1997] showed further examples exhibiting a similar asymmetry. A further statistical study of all 130.4-nm images from September 1981 to February 1982 was performed, but it was not possible to separate the influence of increasing magnetic activity from the analysis, as large values of B_Y were found to be well correlated with large values of AE [*Immel*, 1998].

[12] Numerical experiments using model simulations might offer a solution to this important scientific question, since the thermospheric compositional response to the convection patterns for different IMF B_Z and B_Y can be studied in isolation in a model. However, to date, no first-principles modeling has been performed to test the idea of IMF B_Y compositional effects. In this paper, we use a first-principles model to determine the effect of the IMF B_Y component on the compositional response of the high-latitude thermosphere. The model results indicate that the IMF B_Y component has a strong effect on composition. However, the effect is opposite from that suggested by *Immel et al.* [1997], thus requiring an alternative explanation for the asymmetries illustrated by Figure 1.

2. Thermosphere Ionosphere Mesosphere Electrodynamics General Circulation Model

[13] This study uses a fully coupled three-dimensional (3-D) global model of the ionosphere-thermosphere system, called the Thermosphere Ionosphere Mesosphere Electrodynamics General Circulation Model (TIMEGCM) with heritage in the long line of global models developed at the National Center for Atmospheric Research (NCAR). Thermospheric General Circulation Models (TGCMs) were developed by NCAR beginning in the early 1980s to study the global temperature, circulation, and chemical structure of the thermosphere and its response to solar and auroral activity. A 3-D coupled thermosphere-ionosphere general circulation model (TI-GCM) was developed by *Roble et al.* [1988] and extended to include self-consistent electrodynamic interactions (TIE-GCM) between the ionosphere and

Figure 2. Variations in the northern high-latitude convection patterns obtained from the *Heelis et al.* [1982] model for three values of IMF B_Y, and moderate storm conditions. Geographic/solar local time coordinates; perimeter latitude 42.5°N. Ion velocities at 200km are superposed.

Figure 3. High-latitude total mass density (g cm^{-3}) structure at 140 km altitudes, obtained from the diurnally reproducible runs driven by the corresponding convection patterns in Figure 2. The superposed vectors represent neutral wind flows at 140 km. Perimeter latitude 42.5°N.

thermosphere [*Richmond et al.*, 1992]. The model now extends down to 30 km to include the mesosphere and upper stratosphere and is known as TIME-GCM [*Roble and Ridley*, 1994]. It predicts winds, temperatures, major and minor composition, electron densities, and electrodynamic quantities globally from 30 km to about 600 km altitude. The standard NCAR model uses a fixed geographic grid with a 5° × 5° horizontal resolution, and a vertical resolution of a quarter pressure scale height. (Recent versions of the TIMEGCM can also be run with a 2.5° horizontal resolution). The model time-step is typically 2−3 min, but rapid changes and storms usually require 1 min time steps to maintain model stability.

[14] The codes were initially developed at NCAR for a CRAY Supercomputer environment. Recently, the TIME-GCM code was ported to Southwest Research Institute (SwRI) where it now runs in a distributed parallel computing environment [*Crowley et al.*, 1999b; *Freitas and Crowley*, 1999]. The new code runs on the SwRI Beowulf cluster, consisting of 32 high-end PCs, although it can also be run on a single PC.

[15] The NCAR TIME-GCM has played an important role in understanding the characteristics of the upper atmosphere. An important part of the TIMEGCM success has resulted from its detailed input specification. The inputs required by the model include the solar flux at 57 key wavelengths, parameterized by the F10.7 flux. Typically, the F10.7 flux is available once per day, so the effects of short-term solar variability such as flare effects are not captured with any fidelity. However, day-to-day variability and longer-term effects like the 27-day solar rotation effect and 11-year solar cycle are well reproduced.

[16] Other inputs required by the TIME-GCM include high-latitude particle precipitation and electric fields that permit the model to simulate the response to magnetic activity. *Roble and Ridley* [1987] developed an analytical formulation of the auroral oval and introduced the use of the Heelis convection model [*Heelis et al.*, 1982]. The Heelis model provided an analytical formulation for the shape of the potential pattern, including distortions from the effect of the IMF B_Y component. The magnitude of the potential has to be specified and has often been estimated from an empirical relationship with the Kp or hemispheric power (Hp) index. More recently, the magnitude of the potential has been obtained from the *Weimer* [1996] empirical model or from the Assimilative Mapping of Ionospheric Electrodynamics (AMIE) technique of *Richmond and Kamide* [1988]. Other global models have used Heppner-Maynard potential patterns [*Heppner and Maynard*, 1987].

3. Results

[17] In this paper we present the results of numerical experiments for equinox solar maximum using the NCAR-TIMEGCM to simulate moderate geomagnetic

Figure 4. High-latitude total mass density (g cm^{-3}) structure at 200 km altitudes, obtained from the diurnally reproducible runs driven by the corresponding convection patterns in Figure 2. The superposed vectors represent neutral wind flows at 200 km. Perimeter latitude 42.5°N.
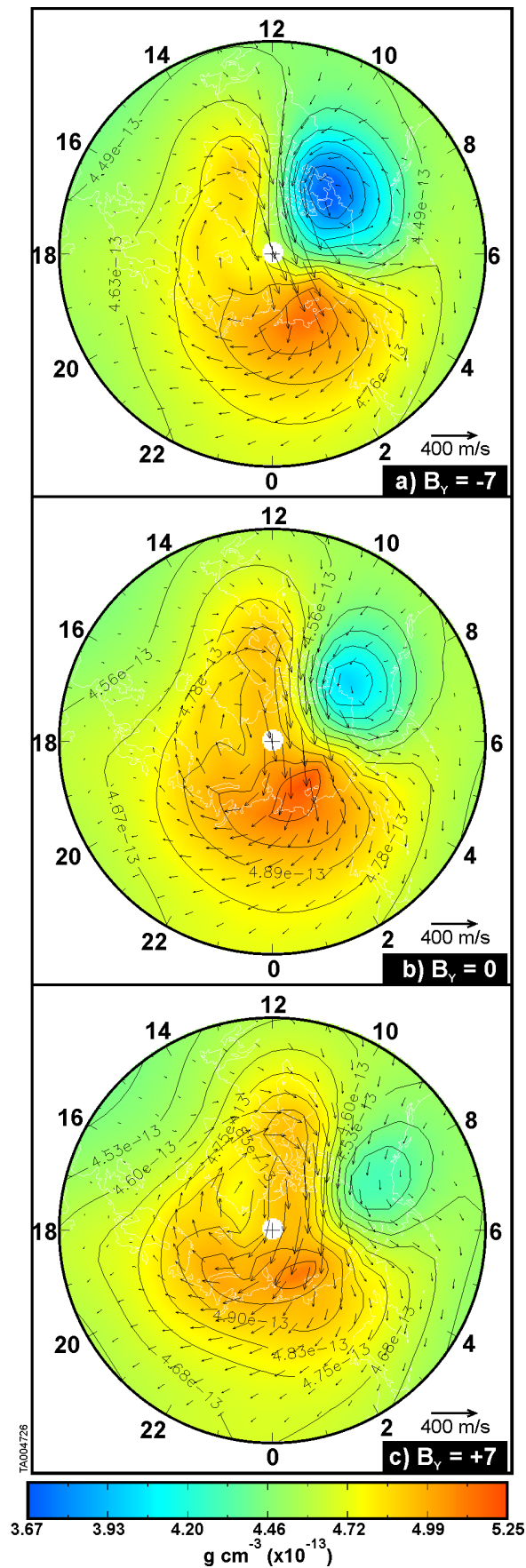
activity. These conditions were simulated using cross-polar cap potentials of 60 kV, with appropriate hemispheric power inputs and are comparable with the moderate activity responsible for the changes observed by DE-1 in Figure 1. To investigate the effect of the IMF B$_Y$ component on the composition, the simulations were repeated with B$_Y$ values of +7, 0, and −7 nT. Each simulation was run to a diurnally reproducible state with the cross-cap potential held constant for 5 days. This selection of runs reveals the development of compositional changes in response to different B$_Y$ conditions. *Crowley et al.* [1996a, 1996b] showed that the behavior of neutral density cells is quite different above a transition height of about 170 km and that the density cell structure decays above about 350 km. Therefore in this paper we examine composition results at both 140 km and 200 km. While we present the results of simple numerical experiments here, the corresponding results for more realistic simulations with time-varying inputs will be presented in another paper by *Immel et al.* [2006, hereinafter referred to as Paper 2].

3.1. Variations in the High-Latitude Convection Pattern

[18] Figure 2 summarizes the variations in the northern high-latitude convection patterns obtained using the *Heelis et al.* [1982] model for three values of IMF B$_Y$ and moderate storm conditions (fixed cross-cap potential of 60 kV). The value of IMF B$_Y$ increases sequentially with each panel down the page from −7 nT to +7 nT. The contours in the figure represent potential patterns for each condition at 1700 UT, with ion-drift vectors at 200 km superposed. The outer latitude of the figures is 42.5°N. At 1700 UT, the magnetic pole and convection pattern are displaced onto the dayside of the dawn-dusk meridian, but the pattern precesses around the geographic pole as a function of UT, as discussed in detail by *Crowley et al.* [1996a, 1999a]. The main effect of changing the IMF B$_Y$ component in the *Heelis et al.* [1982] model is to rotate the angle of flow across the polar region. So for B$_Y$ = −7 nT, the flow is in the noon-midnight meridian, but for B$_Y$ = 0 and +7 nT, it is rotated clockwise by approximately 15° and 30°, respectively. This change in B$_Y$ also rotates the local time of entry on the dayside from about 12–10 SLT. There is also a small increase in the area covered by the dusk cell as B$_Y$ becomes more positive. In each case, the potential difference is split ∼55%:45% between the dusk and dawn cells. These patterns were used to drive the first-principles thermosphere-ionosphere model to diurnally reproducible conditions.

3.2. Density and Composition Variations

[19] The morphology of the total neutral mass density at high latitudes for B$_Y$ = 0 was summarized in section 1. Figures 3 and 4 illustrate the IMF B$_Y$ response of the
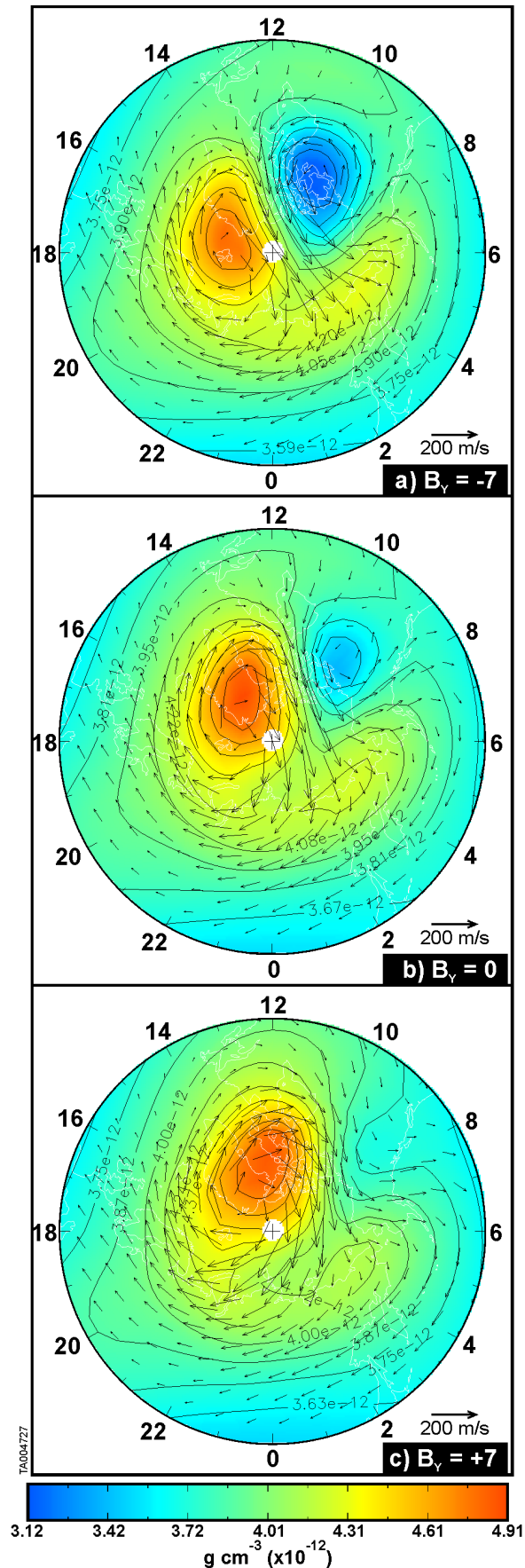
density structure at 140 km and 200 km altitudes, respectively, obtained from the diurnally reproducible runs driven by the corresponding 60 kV convection patterns in Figure 2. The superposed vectors represent neutral wind flows at 140 km and 200 km, respectively. Again, the outer latitude of the figures is 42.5°N. The IMF B$_Y$ increases down the page from −7 nT to +7 nT. Note we only show the density structure for a single (1700) UT. Figure 3 shows that for 140 km, for all three values of the IMF B$_Y$, there are only two well-formed density cells at this altitude (a low- and high-density cell on the dayside), with a hint of a third (high-density) cell in the midnight sector, as expected.

[20] As the IMF B$_Y$ component changes from +7 nT to −7 nT, the clockwise rotation of potential patterns and corresponding ion velocities (see Figure 2) is expected to influence the density structure because the density cells are driven by high-latitude momentum forcing. Figure 3 confirms that the density cells do rotate in local time like the ion convection cells, as the IMF B$_Y$ component changes. The rotation is evident in both the evening and morning cells and in the rotation of the antisunward polar cap neutral wind vectors. The contrast between the afternoon and morning cells also appears to depend on the IMF B$_Y$ component. In particular the morning cell is much better defined for B$_Y$ = −7 nT than for B$_Y$ = +7 nT. For B$_Y$ = −7 nT, the morning cell is depleted by about 30% relative to the evening cell, while for B$_Y$ = +7 nT, it is only depleted by about 20%. The depletion of mass density in the morning cell is correlated with the development of the anticlockwise neutral wind gyre, and in the case of B$_Y$ = +7 nT, the morning gyre is not well developed and the density cell is weak. The reason for the lack of development is the balance of forces at the different local times, but further discussion is outside the scope of the current paper.

[21] Figure 4 shows the corresponding density cell structure with winds for 200 km altitude. The morning (low) and noon (high) density cells are evident in each panel, but the additional high-density cell in the midnight sector is significantly enhanced relative to 140 km (Figure 3), as found by *Crowley et al.* [1996a, 1996b]. In each case, the noon and midnight high-density cells are separated by a slightly lower-density region at the center of the evening neutral wind gyre. This represents the onset of an antibaric flow regime [*Schoendorf et al.*, 1996a] and the formation of a low-density cell that would intensify if the potential were increased further. What is new in Figures 3 and 4 is the rotation of the cell pattern as B$_Y$ changes from +7 nT to −7 nT. The effect of the IMF B$_Y$ component is to rotate the cell structure in the clockwise direction (earlier local times) for increasingly positive B$_Y$. This mimics the rotation of the convection pattern described in Figure 2. For the 200 km case, the morning gyre and corresponding density cell are

Figure 5. High-latitude mass density (g cm^{-3}) of molecular nitrogen at 140 km altitudes, obtained from the diurnally reproducible runs driven by the corresponding convection patterns in Figure 2. The superposed vectors represent neutral wind flows at 140 km. Perimeter latitude 42.5°N.

Figure 6. High-latitude mass density (g cm^{-3}) of molecular nitrogen at 200 km altitudes, obtained from the diurnally reproducible runs driven by the corresponding convection patterns in Figure 2. The superposed vectors represent neutral wind flows at 200 km. Perimeter latitude 42.5°N.
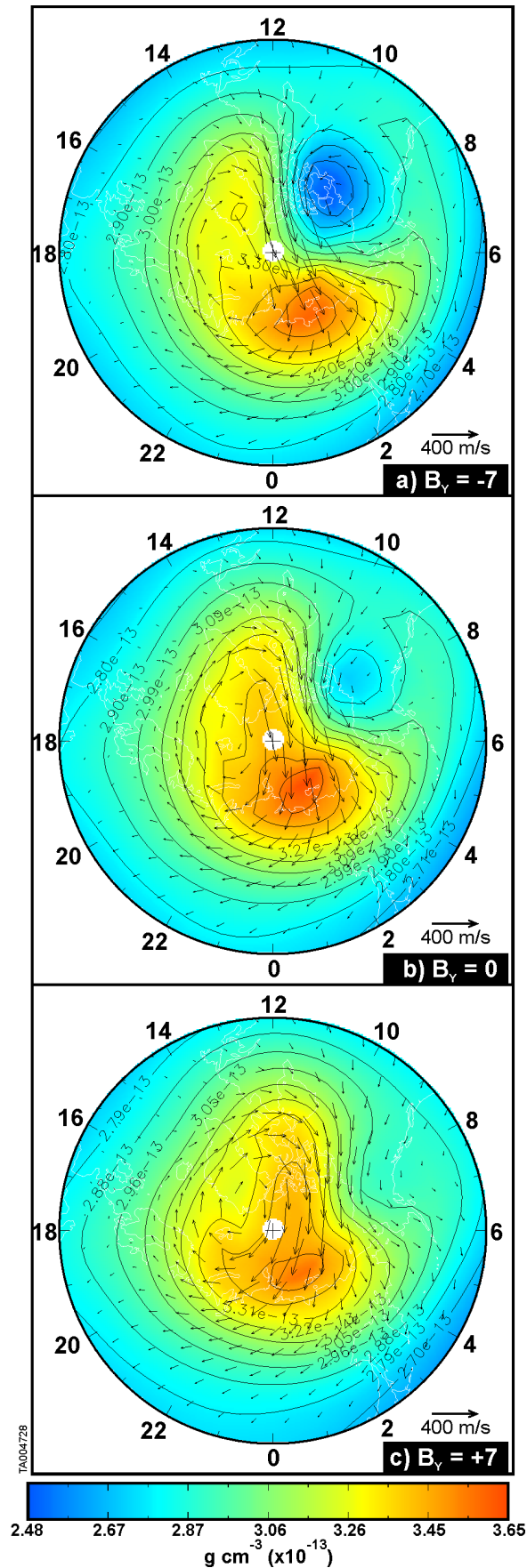
again clearer for the $B_Y = -7$ nT case than for $B_Y = +7$ nT. For $B_Y = -7$ nT, the morning cell is depleted by about 25% relative to the midnight cell, while for $B_Y = +7$ nT, it is only depleted by about 13%.

[22] We find that the O and N_2 respond differently to the high-latitude forcing, and their combined effect is what causes the pattern of total density in Figures 3 and 4. Figures 5 and 6 summarize the high-latitude composition structure for molecular nitrogen at 140 and 200 km, respectively. Comparison of Figures 3 and 5 reveals that at 140 km, the N_2 structure is virtually indistinguishable from the structures in the neutral mass density discussed above. The molecular nitrogen structure mimics the density structure at 140 km because the nitrogen represents ~75% of the atmosphere at this altitude. There is also a significant similarity between the density and N_2 structures at 200 km, however, the dayside N_2 cells are not so clear. As the B_Y component goes from negative to positive the nitrogen cell structures rotate to earlier local times, as noted for the density structures.

[23] Figures 7 and 8 depict the corresponding atomic oxygen structure at 140 and 200 km. The atomic oxygen structure is quite different from the N_2 structure, although a clockwise rotation of the structure is again evident as B_Y progresses from −7 to +7 nT. In Figure 7, the dominant feature in the O distribution at 140 km is a depletion throughout the polar region, with a minimum in the dawn sector centered in the anticlockwise wind gyre. For $B_Y = -7$ nT, the density of O in the dawn cell is less than 50% of the midlatitude values. For $B_Y = +7$ nT, the dawn wind gyre is not well-developed and the O density in the gyre is reduced by only about 40% relative to midlatitude values. Unlike the structure in N2, where extra cells form above 170 km [Crowley et al., 1996a], the overall O structure at 200 km (Figure 8) is similar to that for 140 km, containing a single depletion in the dawn sector that extends over the pole.

3.3. Possible UV Signatures of Composition Variations

[24] The brightness of the FUV dayglow is directly related to the ratio of the column integrated concentrations of O and N_2 ($\Sigma O/N_2$) in the thermosphere. The column integrated O/N_2 ($\Sigma O/N_2$) from the TIMEGCM is computed by identifying the altitude above which the N_2 column density is 10^{17} cm^{-2}, and then integrating [O] above that altitude. The ratio of these integrals is plotted as $\Sigma O/N_2$ in Figure 9. Because the atmospheric density decreases exponentially with increasing altitude, the integrated quantity is heavily weighted toward the lower altitudes. The figure shows that the $\Sigma O/N_2$ reaches minimum values of less than 0.5 in a quasi-circular depression in the polar region because O is generally depleted throughout the polar cap. The minimum $\Sigma O/N_2$ occurs on the dawnside of the polar

Figure 7. High-latitude mass density (g cm^{-3}) of atomic oxygen at 140 km altitudes, obtained from the diurnally reproducible runs driven by the corresponding convection patterns in Figure 2. The superposed vectors represent neutral wind flows at 140 km. Perimeter latitude 42.5°N.
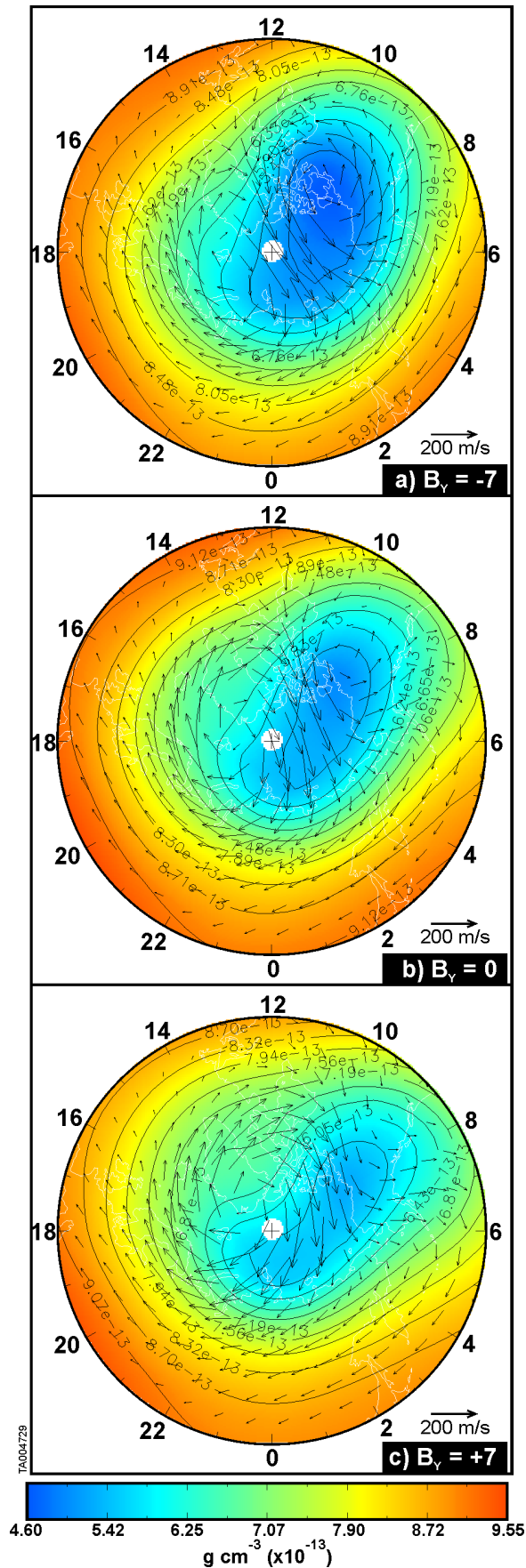
cap, reflecting the fact that O is lowest in that sector. Values of $\Sigma O/N_2$ increase toward midlatitudes, as the density of [O] increases (see Figure 7) while the midlatitude N_2 density is lower than some of the polar values (Figure 5).

[25] There is a distinct B_Y effect in the $\Sigma O/N_2$, most easily seen near the perimeter latitude at 0800 LT, and the entire pattern appears to rotate clockwise by several hours as B_Y changes from -7 to $+7$ nT. The rotation is closely related to the potential pattern rotation. The magnitude of the change in $\Sigma O/N_2$ distribution within the polar cap and auroral zone is large enough to be observed by UV imagers such as those on the DE-1 satellite or by the recent GUVI instrument on the TIMED satellite [*Christensen et al.*, 2003; *Strickland et al.*, 2004; *Meier et al.*, 2005]. In the following section we discuss these results in the light of the *Immel et al.* [1997] predicted B_Y effect.

4. Discussion

[26] *Immel et al.* [1997] suggested that B_Y-positive conditions were more likely to result in $\Sigma O/N_2$ depletions in the morning sector. Although the numerical experiments presented here confirm that the IMF B_Y component has a strong effect on thermospheric density and composition, the modeled B_Y effects are in the opposite direction from the *Immel et al.* [1997] prediction. Specifically, our model results show that (1) the depletion of $\Sigma O/N_2$ on the morningside is 10–20% stronger for B_Y-negative than for B_Y-positive conditions (Figure 9), and (2) the deepest $\Sigma O/N_2$ depletions occur later in the morning sector as the IMF-B_Y becomes increasingly negative. In this paper we only presented results for $B_Y = -7$, 0, and $+7$ nT, but in other simulations we tested larger values of B_Y and found that the rotation in local time becomes even greater as B_Y increases.

[27] The DE-1 observations in Figure 1 depicted relative changes of $\Sigma O/N_2$ compared with quiet time conditions. Therefore in Figure 10 we represent the modeled $\Sigma O/N_2$ from Figure 9 as the percentage change of $\Sigma O/N_2$ relative to quiet time (30 kV potential, $B_Y = 0$) values. While the maxima and minima of the density and composition cells occurred in the polar cap, the largest relative changes in $\Sigma O/N_2$ occurred at auroral and midlatitudes on the morningside. In these numerical experiments with moderate forcing of 60 kV potentials, relative $\Sigma O/N_2$ depletions of more than 30% reach as far as 50 degrees latitude for all three cases, showing that even moderate climatological forcing such as that used in these numerical experiments produces significant and measurable depletions of $\Sigma O/N_2$ throughout the morning (0600–1200 LT) sector, regardless of the sign of B_Y.

[28] In Figure 1, conditions on Day 267 (B_Y-positive) produced depletions of 30% in the morning sector extending to 50 degrees latitude (south of Alaska). It is therefore

Figure 8. High-latitude mass density (g cm^{-3}) of atomic oxygen at 200 km altitudes, obtained from the diurnally reproducible runs driven by the corresponding convection patterns in Figure 2. The superposed vectors represent neutral wind flows at 200 km. Perimeter latitude 42.5°N.
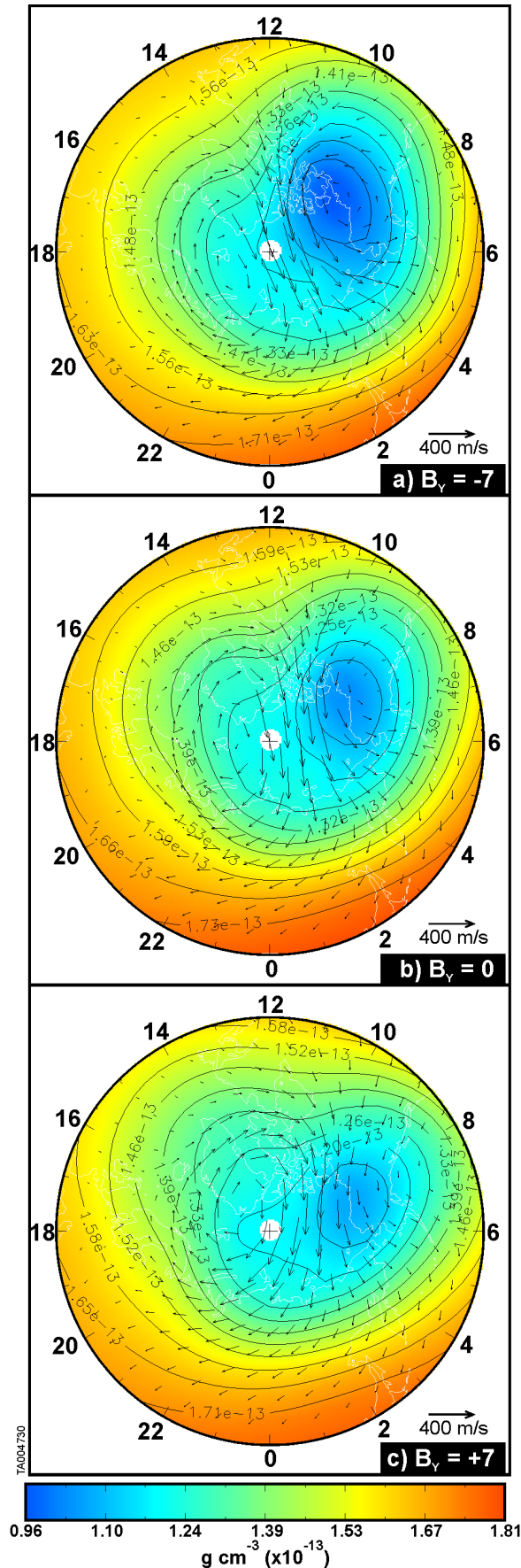
particularly satisfying that in Figure 10c, the maximum relative depletion for $B_Y = +7$ occurs to the south of Alaska, exactly where the DE-1 image measures it. Thus Figure 10c appears to be very comparable with the observations at 1700 UT for Day 267 shown in Figure 1.

[29] Comparison of the three panels in Figure 10 indicate that the relative depletion in $\Sigma O/N_2$ is rotated to later times for more negative IMF-B_Y, which is consistent with rotation effects noted above for density, composition, and winds. Therefore in Figure 1, the DE-1 image for $B_Y = 0$ conditions on Day 279 might be expected to show a larger depletion at later local times than that observed on Day 267, where B_Y was strongly positive. However, the observed morningside depletion on Day 279 was small. Thus the DE-1 observation on Day 279 appears anomalous relative to the numerical experiments presented here. We therefore suggest that some factor other than IMF By was responsible for the lack of observed depletion on Day 279.

[30] In spite of the similar AE indices on the 2 days, there are fundamental differences between the geophysical conditions on Days 267 and 279. The lower panels of Figure 1 reveal that B_Z and B_Y had much larger values on Day 267 than Day 279; in particular, the B_Y component remained near +10 nT for most of Day 267, while the corresponding B_Y component was close to zero throughout day 279, with a brief positive excursion between 1000 and 1400 UT. Perhaps more significantly, B_Z was -5 to -10 nT for several hours on Day 267, whereas for most of Day 279, B_Z was generally small and only reached -5 nT for an hour before the image was taken. In general, stronger Bz southward values correspond to stronger energy input into the magnetosphere and ionosphere. In addition to IMF values, the Epsilon parameter [*Akasofu*, 1981], which is a measure of the input solar wind power available for subsequent magnetospheric energization, was shown in Figure 1. The values of Epsilon were determined using the 5-min average IMF values shown in the figure, and the hourly solar wind speeds interpolated at 5-min intervals. Epsilon is plotted on a logarithmic scale and is consistently greater on Day 267 than on Day 279. Taken together, these data suggest that the main difference between the thermospheric composition disturbances on Day 267 and Day 279 may have been the deposition of more energy on Day 267, rather than the IMF B_Y component.

[31] On the other hand, we could also say the numerical experiments themselves appear anomalous relative to the observed response of the thermospheric system on Day 279. The simple numerical experiments presented here may have omitted some detail of the convection pattern response to IMF-B_Y, or a mechanism involving the interaction of time-varying quantities. For example, rapid changes in the high-latitude inputs were not captured in these simulations. It is therefore of interest to perform more realistic simulations of the intervals observed by the DE-1 satellite. Such realistic
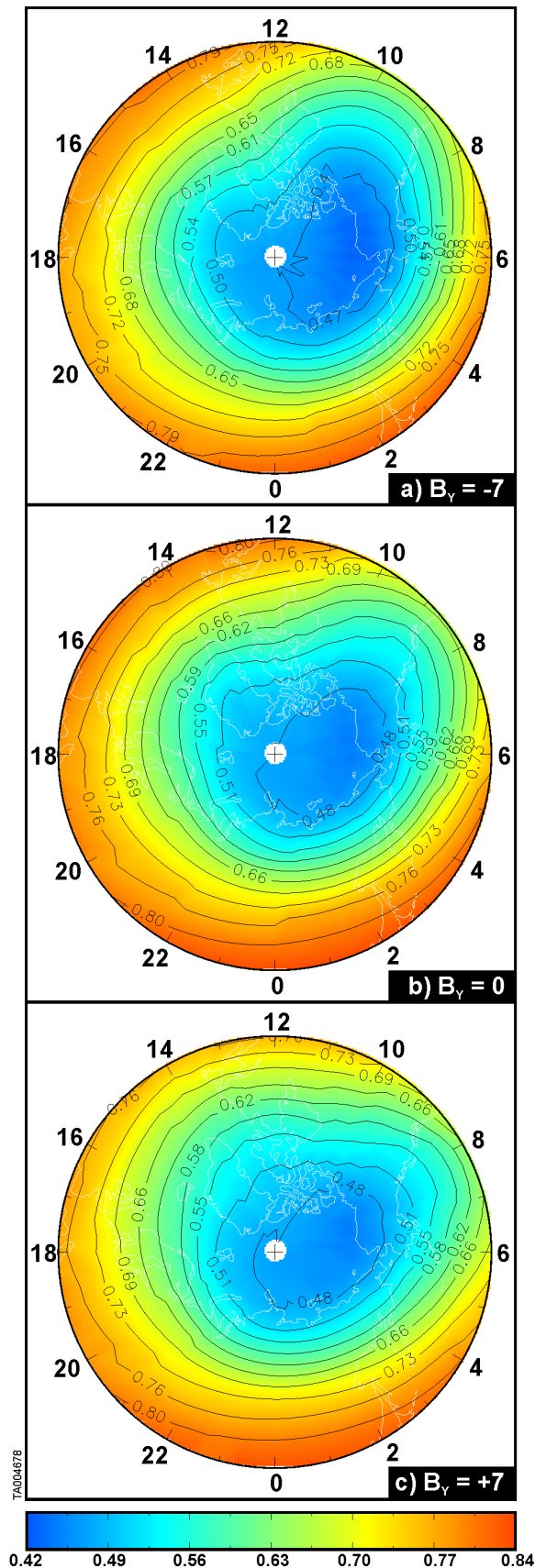
Figure 9. Column integrated O/N$_2$ ratio corresponding to the previous figures, with the height integration above $\Sigma N_2 = 10^{17} cm^{-2}$.

simulations of the DE period are discussed in Paper 2 [*Immel et al.*, 2006].

[32] The *Immel et al.* [1997] paper argued that cross-polar cap winds would be more likely to carry depleted air out of the polar cap and into the morning sector for B$_Y$-positive. However, the cross polar cap winds shown in this paper (e.g., Figures 7 and 8) were always rotated anticlockwise to later local times for B$_Y$-negative. Such a rotation might be expected because the high-latitude winds are driven by the convection, which also rotates anticlockwise to later local times for B$_Y$-negative (see Figure 2). We note that the convection cells used in these numerical experiments contained mainly a rotational response to the IMF-B$_Y$ component. The convection patterns also show the dawn (dusk) cell becoming more dominant as By becomes more negative (positive), as discussed in section 1; however, in practice the Heelis model may underestimate this change in relative size. We note that the auroral zone neutral winds in our simulations do not reproduce the observed effect of *Rees et al.* [1986], in which they transition from westward to eastward in the midnight sector 2 hours earlier for B$_Y$ negative than for B$_Y$ positive. Such an effect may be caused by permitting the dusk convection cell to grow more relative to the dawn cell when B$_Y$ is positive. However, a diminishing in the size of the dawn convection cell for By positive will likely reduce the morningside composition changes even more than shown in Figures 5–8 and are therefore unlikely to produce a stronger depletion in the morning sector like that invoked by *Immel et al.* [1997] to explain the observations in Figure 1. A modeling study will be performed in the near future to test the effects of greater relative changes in the size of the dawn and dusk convection cells.

5. Conclusion

[33] In this paper we have confirmed that the IMF B$_Y$ component has a significant effect on thermospheric neutral density and composition. In particular, a change from B$_Y$-negative to B$_Y$-positive causes a clockwise rotation of the potential pattern, which drives a corresponding rotation in the wind and in density and composition distributions. The height-integrated O/N$_2$ ratio ($\Sigma O/N_2$) for all these conditions exhibits a minimum in the morning high latitudes, extending over the pole, but our model results show that (1) the depletion of $\Sigma O/N_2$ on the morningside is 10–20% stronger for B$_Y$-negative than for B$_Y$-positive conditions; (2) the deepest $\Sigma O/N_2$ depletions occur later in the morning sector as the IMF-B$_Y$ becomes increasingly negative; (3) while the maxima and minima of the density and composition cells occurred in the polar cap, the largest relative changes in $\Sigma O/N_2$ occurred at auroral and midlatitudes on the morningside; and (4) the *Immel et al.* [1997] suggestion that B$_Y$ positive would cause greater penetration into the morning sector is opposite from the effect in our simulations.

[34] The numerical experiments presented here have permitted the separation of different factors, such as IMF and magnetic activity levels that were confounded in the DE-1 data analysis of *Immel et al.* [1997]. Our numerical experiments using climatological inputs produced significant depletions that are comparable with those measured
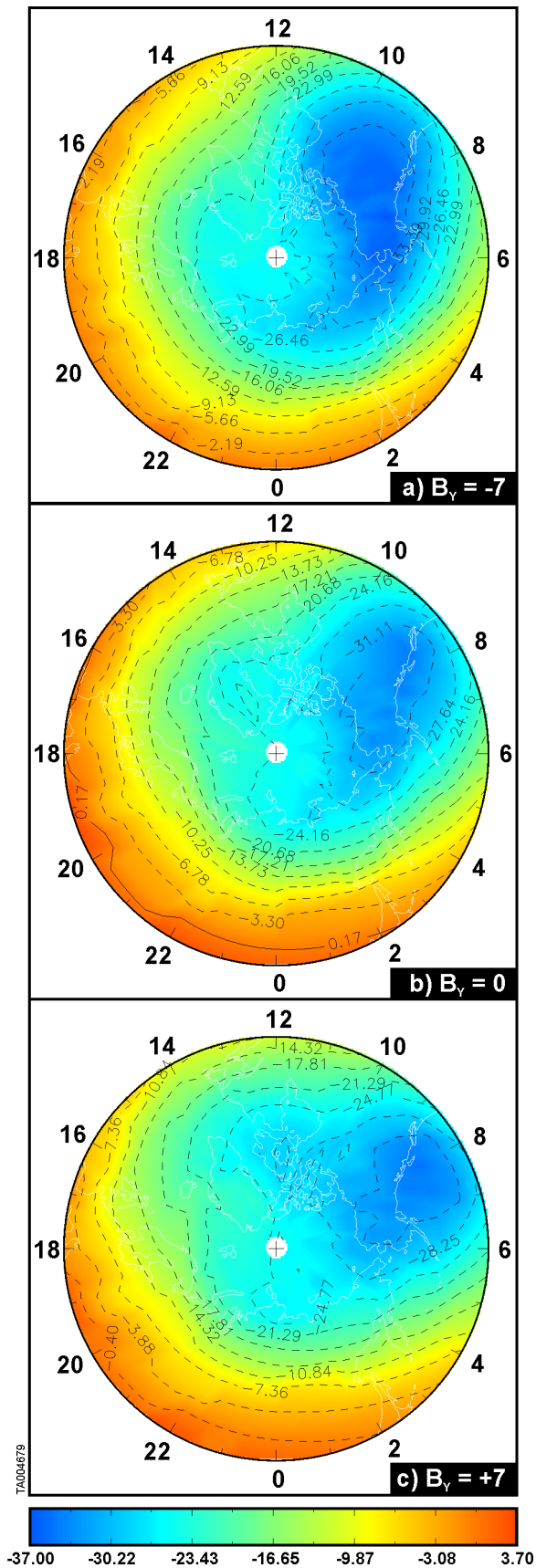
Figure 10. Percentage depletion of $\Sigma O/N_2$ from Figure 9 relative to quiet time (30 kV potential, B$_Y$ = 0) values.

by DE-1. However, larger effects are predicted for B$_Y$ $\sim$ 0 and B$_Y$ negative than for B$_Y$ positive conditions, in contrast to the DE-1 observations on Days 267 and 279. Whether this is because of the model, model inputs, or because of a geophysical effect on Day 279 remains to be seen. However, the larger Epsilon parameter and southward IMF-B$_Z$ on Day 267 suggest that the main difference between the 2 days may be the larger amount of energy input driving the thermosphere on Day 267, rather than the difference in the B$_Y$ component.

[35] Further work needs to be performed on this problem, using data and model simulations that take advantage of modern capabilities. In recent years, models of the coupled thermosphere-ionosphere system, such as the TIMEGCM used here, have been developed that identify the major contributors to the aeronomy of the upper atmosphere. Relatively little work has been done to validate the global models by comparing realistic simulations with large iono-sphere-thermosphere data sets or to establish what are the shortcomings of the models and how they can be improved. Therefore studies such as the one presented here are extremely useful and valuable.

[36] Modeling of thermospheric variability is challenging because our knowledge of the inputs is incomplete, and their specification requires copious amounts of data. It is now possible to specify the thermospheric drivers with unprecedented accuracy: for example, the Assimilative Mapping of Ionospheric Electrodynamics (AMIE) technique [*Richmond and Kamide*, 1988; *Richmond et al.*, 1992] is an inversion method that can take data from a wide array of sources, including satellites, radar, and ground-based magnetometers. In principle, AMIE can produce a realistic representation of the high-latitude electrodynamic state at a particular time; however, gathering the appropriate electrodynamics input data (if it exists) is extremely labor-intensive. Eventually, we plan to simulate the DE-1 period in more detail using more realistic time-varying high-latitude potential patterns from AMIE, to investigate what factors might have caused the $\Sigma O/N_2$ depletions on Day 267 to be so much greater than those observed on Day 279.

[37] In the present era, ultraviolet imagers are currently in orbit on the NASA-IMAGE and TIMED satellites and the Air Force DMSP satellites. For example, the Global Ultraviolet Imager (GUVI) on the TIMED satellite uses five different wavelength bands to deduce various atmospheric properties. It uses the ratio of 1356Å to LBH brightness to estimate $\Sigma O/N_2$ on the Earth's disk [*Christensen et al.*, 2003; *Strickland et al.*, 2004; *Meier et al.*, 2005]. Also, when observing the limb GUVI can derive vertical profiles of the O, O$_2$, and N$_2$ concentration, which can then be used to derive $\Sigma O/N_2$. A similar instrument, the Special Sensor Ultraviolet Spectrographic Imager (SSUSI) was launched on a DMSP satellite in the fall of 2003. These instruments are providing new data sets with which to study the effect of IMF variations on the high- and middle-latitude composition. It will be possible to utilize these high-quality data to further investigate the effect of IMF orientation on thermospheric composition.

References

Akasofu, S. I. (1981), Energy coupling between the solar wind and the magnetosphere, *Space Sci. Rev.*, *28*, 121–190.

Buonsanto, M. J. (1999), Ionospheric storms—A review, *Space Sci. Rev.*, *88*, 563–601.

Burns, A. G., T. L. Killeen, and R. G. Roble (1991), A theoretical study of thermospheric composition perturbations during an impulsive geomagnetic storm, *J. Geophys. Res.*, *96*, 14,153–14,167.

Burns, A. G., T. L. Killeen, G. R. Carignan, and R. G. Roble (1995a), Large enhancements in the O/N$_2$ ratio in the evening sector of the winter hemisphere during geomagnetic storms, *J. Geophys. Res.*, *100*, 14,661–14,671.

Burns, A. G., T. L. Killeen, W. Deng, G. R. Cargnan, and R. G. Roble (1995b), Geomagnetic storm effects in the low-to-middle-latitude upper thermosphere, *J. Geophys. Res.*, *100*, 14,673–14,691.

Caspers, T., and G. W. Prölss (1999), Thermospheric density cells in high latitudes, *Adv. Space Res.*, *24*, 1433–1437.

Christensen, A. B., et al. (2003), Initial observations with the Global Ultraviolet Imager (GUVI) in the NASA TIMED satellite mission, *J. Geophys. Res.*, *108*(A12), 1451, doi:10.1029/2003JA009918.

Craven, J. D., A. C. Nicholas, L. A. Frank, D. J. Strickland, and T. J. Immel (1994), Variations in FUV dayglow after intense auroral activity, *Geophys. Res. Lett.*, *21*, 2793–2796.

Crowley, G., B. A. Emery, R. G. Roble, H. C. Carlson, and D. J. Knipp (1989a), Thermospheric dynamics during the equinox transition study: 1. Model simulations for Sept 18 and 19, 1984, *J. Geophys. Res.*, *94*, 16,925–16,944.

Crowley, G., et al. (1989b), Thermospheric dynamics during the equinox transition study of September 1984: 2. Validation of the NCAR-TGCM, *J. Geophys. Res.*, *94*, 16,945–16,960.

Crowley, G., P. S. Cannon, C. G. Dozois, B. W. Reinisch, and J. Buchau (1992), Polar cap convection for Bz northward, *Geophys. Res. Lett.*, *19*, 657–660.

Crowley, G., J. Schoendorf, R. G. Roble, and F. A. Marcos (1995), Satellite observations of neutral density cells in the lower thermosphere at high latitudes, in *The Upper Mesosphere and Lower Thermosphere: A Review of Experiment and Theory, Geophys. Monogr. Ser.*, vol. 87, edited by R. M. Johnson and T. L. Killeen, pp. 339–348, AGU, Washington, D. C.

Crowley, G., J. Schoendorf, R. G. Roble, and F. A. Marcos (1996a), Cellular structures in the high-latitude thermosphere, *J. Geophys. Res.*, *101*, 211–223.

Crowley, G., J. Schoendorf, R. G. Roble, and F. A. Marcos (1996b), Neutral density cells in the lower thermosphere at high latitudes, *Adv. Space Res.*, *18*(3), 69–74.

Crowley, G., A. Ridley, D. Winningham, R. Frahm, and J. Sharber (1999a), On the hemispheric symmetry in thermospheric nitric oxide, *J. Geophys. Res.*, *26*, 1545–1548.

Crowley, G., C. J. Freitas, A. Ridley, D. Winningham, R. G. Roble, and A. D. Richmond (1999b), Next generation space weather specification and forecasting model, paper presented at Ionospheric Effects Symposium, Off. of Naval Res., Alexandria, Va.

Doyle, M. A., and W. J. Burke (1983), S3-3 measurements of the polar cap potential, *J. Geophys. Res.*, *88*, 9125–9133.

Freitas, C. J., and G. Crowley (1999), Space weather simulation on networks of workstations, paper presented at Forum on Parallel Computing Methods, International Mechanical Engineering Congress and Exposition, ASME, Nashville, Tenn.

Fuller-Rowell, T. J., M. V. Codrescu, R. J. Moffett, and S. Quegan (1994), Response of the thermosphere and ionosphere to geomagnetic storms, *J. Geophys. Res.*, *99*, 3893–3914.

Fuller-Rowell, T. J., M. V. Codrescu, H. Rishbeth, R. J. Moffett, and S. Quegan (1996), On the seasonal response of the thermosphere and ionosphere to geomagnetic storms, *J. Geophys. Res.*, *101*, 2343–2353.

Hedin, A. E., et al. (1977), A global thermospheric model based on mass spectrometer and incoherent scatter data MSIS: 1. N$_2$ density and temperature, *J. Geophys. Res.*, *82*, 2139–2147.

Heelis, R. A. (1984), The effects of interplanetary magnetic field orientation on dayside high-latitude ionospheric convection, *J. Geophys. Res.*, *89*, 2873.

Heelis, R. A., J. K. Lowell, and R. W. Spiro (1982), A model of the high latitude ionospheric convection pattern, *J. Geophys. Res.*, *87*, 6339–6345.

Heppner, J. P. (1972), Polar-cap electric field distributions related to the interplanetary magnetic field direction, *J. Geophys. Res.*, *77*, 4877.

Heppner, J. P., and N. C. Maynard (1987), Empirical high-latitude electric field models, *J. Geophys. Res.*, *92*, 4467–4489.

Hernandez, G., F. G. McCormac, and R. W. Smith (1991), Austral thermospheric wind circulation and interplanetary magnetic field orientation, *J. Geophys. Res.*, *96*, 5777–5783.

Immel, T. J. (1998), Studies of compositional variations in the thermosphere and ionosphere using far-ultraviolet images from DE 1, thesis paper, Univ. of Alaska, Fairbanks, Ala.

Immel, T. J., J. D. Craven, L. A. Frank, and J. B. Sigwarth (1997), Variations in Earth's FUV dayglow within the polar caps, *Eos Trans. AGU*, *78*(46), Fall Meet. Suppl., F520.

Immel, T. J., G. Crowley, and J. D. Craven (2001), Dayside enhancements of thermospheric O/N$_2$ following a magnetic storm onset, *J. Geophy. Res.*, *106*, 15,471–15,488.

Immel, T. J., G. Crowley, and J. D. Craven (2006), The importance of high latitude inputs in correctly modeling the magnitude and extend of thermospheric storms, *Adv. Space Res.*, in press.

Killeen, T. L., Y.-I. Won, R. J. Niciejewski, and A. G. Burns (1995), Upper thermosphere winds and temperatures in the geomagnetic polar cap: Solar cycle, geomagnetic activity, and interplanetary magnetic field dependences, *J. Geophys. Res.*, *100*, 21,327–21,342.

Mayr, H. G., and H. Volland (1973), Magnetic storm characteristics of the thermosphere, *J. Geophys. Res.*, *78*, 2251.

McCormac, F. G., T. L. Killeen, E. Gombosi, P. B. Hays, and N. W. Spencer (1985), Configuration of the high-latitude thermosphere neutral circulation for IMF B$_Y$ negative and positive, *J. Geophys. Res.*, *12*, 155–158.

McCormac, F. G., T. L. Killeen, and J. P. Thayer (1991), The influence of IMF B$_Y$ on the high-latitude thermospheric circulation during northward IMF, *J. Geophys. Res.*, *96*, 115–128.

Meier, R. R., R. Cox, D. J. Strickland, J. D. Craven, and L. A. Frank (1995), Interpretation of Dynamics Explorer far UV images of the quiet time thermosphere, *J. Geophys. Res.*, *100*, 5777–5794.

Meier, R. R., G. Crowley, D. J. Strickland, A. B. Christensen, L. J. Paxton, and D. Morrison (2005), First look at the 20 November 2003 superstorm with TIMED/GUVI, *J. Geophys. Res.*, *110*, A09S41, doi:10.1029/2004JA010990.

Miller, N. J., L. H. Brace, N. W. Spencer, and G. R. Carignan (1990), DE 2 observations of disturbances in the upper atmosphere during a geomagnetic storm, *J. Geophys. Res.*, *95*, 21,017–21,031.

Prölss, G. W. (1980), Magnetic storm associated perturbations of the upper atmosphere: Recent results obtained by satellite-borne gas analyzers, *Rev. Geophys.*, *18*, 183–202.

Rees, D., R. Gordon, T. J. Fuller-Rowell, M. Smith, G. R. Carignan, T. L. Killeen, P. B. Hays, and N. W. Spencer (1985), The composition, structure, temperature and dynamics of the upper thermosphere in the polar regions during October to December 1981, *Planet. Space Sci.*, *33*, 617–666.

Rees, D., T. J. Fuller-Rowell, R. Gordon, M. F. Smith, N. C. Maynard, J. P. Heppner, N. W. Spencer, L. Wharton, P. B. Hays, and T. L. Killeen (1986), A theoretical and empirical study of the response of the high latitude thermosphere to the sense of the "Y" component of the interplanetary magnetic field, *Planet. Space Sci.*, *34*, 1–40.

Reiff, P. H., R. W. Spiro, and T. W. Hill (1981), Dependence of polar cap potential drop on interplanetary parameters, *J. Geophys. Res.*, *87*, 5260–5266.

Richmond, A. D., and Y. Kamide (1988), Mapping electrodynamic features of the high-latitude ionosphere from localized observations: Technique, *J. Geophys. Res.*, *93*, 5741–5759.

Richmond, A. D., E. C. Ridley, and R. G. Roble (1992), A thermosphere/ionosphere general circulation model with coupled electrodynamics, *Geophys. Res. Lett.*, *19*, 601–604.

Roble, R. G., and E. C. Ridley (1987), An auroral model for the NCAR thermospheric general circulation model (TGCM), *Ann. Geophys., Ser. A*, *5*, 369–382.

Roble, R. G., and E. C. Ridley (1994), A thermosphere-ionosphere-mesosphere-electrodynamics general circulation model (TIME-GCM): Equinox solar minimum simulations (30–500 km), *Geophys. Res. Lett.*, *21*, 417–420.

Roble, R. G., T. L. Killeen, N. W. Spencer, R. A. Heelis, P. H. Reiff, and J. D. Winningham (1988), Thermospheric dynamics during November 21–22, 1981: Dynamics Explorer measurements and thermospheric general circulation model predictions, *J. Geophys. Res.*, *93*, 209–225.

Ruohonemi, J. M., and R. A. Greenwald (1995), Observations of IMF and seasonal effects in high-latitude convection, *Geophys. Res. Lett.*, *22*, 1121–1124.

Schoendorf, J., G. Crowley, and R. G. Roble (1996a), Formation mechanism for thermospheric neutral density cells at high latitudes, *J. Atmos. Terr. Phys.*, *58*, 1769–1781.

Schoendorf, J., G. Crowley, R. G. Roble, and F. A. Marcos (1996b), Neutral density cells in the high latitude thermosphere: morphology for solar maximum deduced from TIGCM simulations, *J. Atmos. Terr. Phys.*, *58*, 1751–1768.

Strickland, D. J., R. E. Daniell, and J. D. Craven (2001), Negative ionospheric storm coincident with DE-1 observed thermospheric disturbance, *J. Geophys. Res.*, *106*, 21,049–21,062.

Strickland, D. J., R. R. Meier, R. L. Walterscheid, A. B. Christensen, L. J. Paxton, D. Morrison, J. D. Craven, and G. Crowley (2004), Quiet-time seasonal behavior of the thermosphere seen in the far ultraviolet dayglow, *J. Geophys. Res.*, *109*, A01302, doi:10.1029/2003JA010220.

Thayer, J. P., T. L. Killeen, F. G. McCormac, C. R. Tschan, J. J. Ponthieu, and N. W. Spencer (1987), Thermospheric neutral wind signatures dependent on the east-west component of the interplanetary magnetic field for Northern and Southern Hemispheres as measured from Dynamics Explorer 2, *Ann. Geophys., Ser. A*, *5*, 363–368.

Weimer, D. R. (1996), A flexible, IMF dependent model of high-latitude electric potential having "space weather" applications, *Geophys. Res. Lett.*, *23*, 2549.

————————————

J. Craven, Geophysical Institute and Physics Department, University of Alaska Fairbanks, Fairbanks, AK 99775, USA.

G. Crowley, Atmospheric and Space Technology Research Associates, 11118 Quail Pass, San Antonio, TX 78249, USA. (gcrowley@astraspace.net)

C. L. Hackert, Southwest Research Institute, 6220 Culebra Road, San Antonio, TX 78238-5166, USA.

T. J. Immel, Space Sciences Laboratory, University of California, Berkeley, Berkeley, CA 94720, USA.

R. G. Roble, High Altitude Observatory, National Center for Atmospheric Research, Boulder, CO 80303, USA.